KINEMATICS ANALYSIS AND EXPERIMENTAL RESEARCH OF DEEP SEA MINING ROBOT

Yun LIU[1,*], Yong JIANG[2]

In this paper, the kinematic mathematical model of the mining robot in the deep sea unstructured terrain environment is established, and the kinematics characteristics of the robot are analyzed theoretically. At the same time, the robot virtual prototype simulation model is set up to simulate the typical conditions of the deep sea environment, and the dynamic characteristic simulation curves of the robot are obtained, so that the prototype of the robot is developed and tested, and the experimental curves of the robot's motion characteristics are obtained. By comparing the simulation curves with the test data, the accuracy of the kinematics mathematical model is verified, therefore, a theoretical reference for the research of deep sea wheeled mining robot kinematics characteristics is provided, which provides the technical support for the development of deep sea mining robot.

Keywords: Deep sea; Mining robot; Kinematics; Virtual simulation

1. Introduction

Deep sea is rich in mineral resources, while the deep-sea terrain environment is complex and changeable. The development of mining robots with good performance, strong obstacle crossing and tolerance performance, and high safety and reliability is the core key to develop the deep-sea technology in various countries [1-3].

The research on the kinematics of wheeled robot is based on the theory of robot manipulator, but it is different from that of fixed base robot. The motion constraint equation of wheeled robot is incomplete, that is, it contains non integrable algebraic equation, and the system coordinates can not be eliminated by the constraint equation. Therefore, in order to describe the system, we have to introduce the number of generalized coordinates more than the system degrees of freedom, which makes the movement, dynamics and control of the wheeled robot much more complex than the robot manipulator [4-6]. In addition, each wheel of the wheeled robot is driven independently, so the problem of synchronous driving of each wheel will affect its controllability.

[1,*] Prof. Yun Liu, College of Mechanical-Electrical and Vehicle Engineering, Weifang University, China; email: wflyun@wfu.edu.cn
[2] Senior eng., Yong Jiang, Beijing General Research Institute of Mining & Metallurgy, China

Since the 1980s, many scholars have studied the motion, dynamics and control of nonholonomic systems such as wheeled robots and exploration vehicles [7,8]. In 1987, P. F. Muir et al. proposed a kinematic modeling method based on coordinate transformation for planar wheeled robots. Since then, many references have established corresponding kinematic models for different types of wheeled robots using the basic idea of this method [9]. Greg McDermott and Mahmoud Tarokh of San Diego State University in the United States have proposed a general kinematic modeling method for articulated robots in three-dimensional rough terrain, in which the position, posture, motion of each joint, wheel sliding, subsidence and other information are comprehensively considered in the model [10]. In the past decade, the deep-sea mining robot technology has been developed rapidly, and countries all over the world have raised the development of deep-sea mining robot technology as a national strategy.

At present, in the field of deep-sea mining robot kinematics research, most of the models established by researchers are limited to the flat and smooth deep-sea terrain environment. These models can only be used to realize the motion control of the walking mechanism in the two-dimensional plane, that is, the translation in the X and Y directions and the rotation around the Z axis, but are not suitable for describing the motion on the rugged three-dimensional deep-sea complex terrain [11,12]. Based on the kinematics research of wheeled robot, a new type of compound wheeled deep-sea mining robot is proposed in this paper, whose obstacle surmounting, mobility and trafficability are greatly improved. Through in-depth analysis of the kinematics characteristics of deep-sea wheeled mining robot, a kinematics mathematical model based on D-H coordinate transformation is established, which can better describe the motion characteristics of the robot in the deep-sea three-dimensional rough terrain. At the same time, the kinematics theoretical model is verified by virtual prototype simulation and principle prototype test, which provides theoretical reference for the research on kinematics characteristics of deep-sea wheeled mining robot, and provides technical support for the development of deep-sea mining robot.

2. Structure design of the deep sea composite wheeled mining robot

Deep sea composite wheel mining robot mainly consists of four parts: mechanical system, power system, hydraulic system and control system, as shown in Fig. 1.

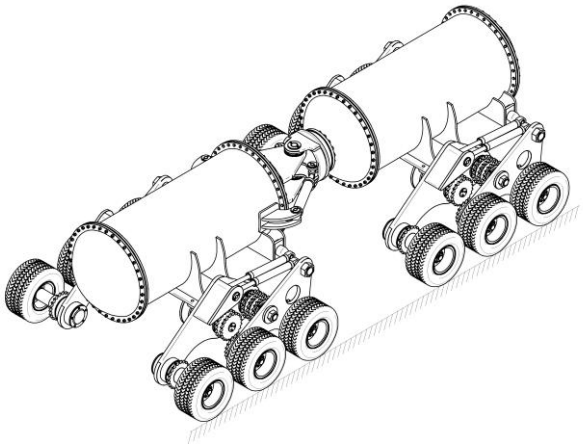

Fig. 1. The deep sea composite wheeled mining robot

Among them, the main structure of the mechanical system is composed of 4 sets of composite wheel sets and hinged sealing frame; the power system is composed of waterproof motor, hydraulic pump, hydraulic motor and auxiliary components (as shown in Fig. 2); the hydraulic system is composed of hydrostatic drive system, steering system and obstacle crossing executive system; the control system is mainly composed of power supply module, signal acquisition module and output control module (as shown in Fig. 3).

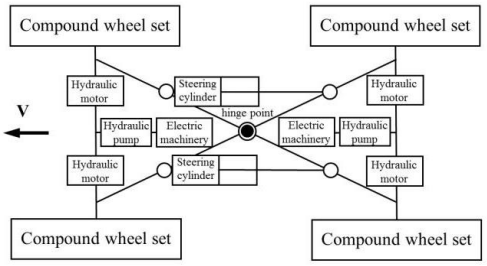

Fig. 2. Power system design

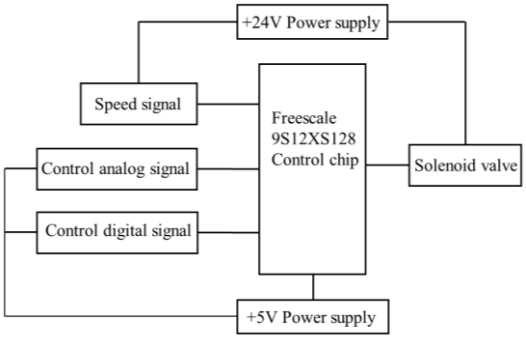

Fig. 3. Control system structure diagram

3. Kinematics analysis of deep sea mining robot

The kinematic model of deep-sea mining robot will establish the relationship between wheel motion and vehicle body, so as to determine the position and posture of the robot in different motion positions. In order to facilitate the modeling, the following assumptions are made: there is no deformation between the wheel and the deep-sea bottom; there is point contact between the wheel and the deep-sea bottom; the geometric center of the contact

point is located at the intersection of the normal of the deep-sea bottom passing through the wheel center and the wheel circumference on the grounding side.

3.1 Establishment and transformation of coordinate system

In order to establish the kinematic model, a series of coordinate systems are established at each joint of the robot according to the D-H coordinate transformation rules, so that the translation and rotation motion relations between the robot joints are described by the homogeneous transformation between the coordinate systems [13,14]. Since the structure of the robot is symmetrical to the left and right, it only needs to represent the coordinate system of one side, as shown in Fig. 4.

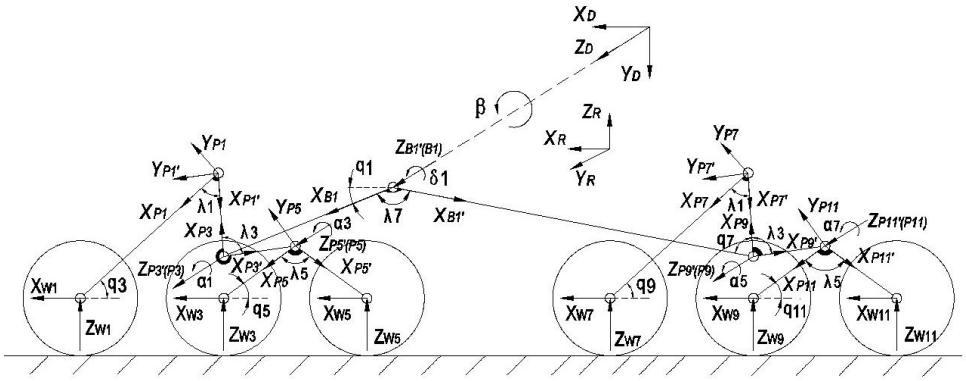

Fig. 4. Left coordinate system of the robot

According to the D-H coordinate transformation rule, θ_i represents the angle of rotation around the Z_{i-1} axis, from X_{i-1} to X_i; d_i represents the distance along Z_{i-1} from the origin of the $i-1$-th coordinate system to the intersection point of Z_{i-1}-axis and X_i-axis; a_i represents the distance along X_{i-1}-axis between the intersection point of Z_{i-1}-axis and X_{i-1}-axis and the origin of X_i-axis; α_i represents the angle of i-coordinate system from Z_{i-1}-axis to Z_i-axis around X_i-axis. According to the above definition and the seabed vehicle motion model, the D-H parameters corresponding to each adjacent coordinate system can be obtained, as shown in Table 1.

Table 1

D-H Coordinate parameters

Coordinate system	θ_i (°)	d_i (mm)	a_i (mm)	α_i (°)
D	$\theta_1 = 0$	0	0	-90
B1	$\theta_2 = \beta + \delta_1 + q_1$	350	0	0
P3	$\theta_3 = q_1 - \lambda_1 - q_3 - \alpha_1$	140	700	0
P1’	$\theta_4 = 180$	0	320	0
P1	$\theta_5 = -\lambda_1$	0	0	0

W1	$\theta_6 = -q_3$	330	710	90
P3’	$\theta_7 = 180 - \lambda_3 + \lambda_1 + q_3 - q_1 + \alpha_1$	0	700	0
P5	$\theta_8 = \lambda_3 + q_1 - q_3 - \lambda_1 - 180$	200	280	0
W3	$\theta_9 = -q_5$	130	340	0
P5’	$\theta_{10} = \lambda_5 + q_1 + \lambda_3 - q_3 - \lambda_1 - 180 + \alpha_3$	200	0	0
W5	$\theta_{11} = -q_5 + \lambda_5$	130	340	90
B1’	$\theta_{12} = q_1 + \lambda_7 + \delta_1 + \beta$	350	0	0
P9	$\theta_{13} = q_7 - 180 - \alpha_5$	140	1800	0
P7’	$\theta_{14} = 180$	0	320	0
P7	$\theta_{15} = -\lambda_1$	0	0	0
W7	$\theta_{16} = -q_9$	330	710	90
P9’	$\theta_{17} = 180 - q_7 - \lambda_3 + \alpha_5$	0	1800	0
P11	$\theta_{18} = \lambda_3 + q_{11} - q_9 - \lambda_1 - 180 - \alpha_7$	200	280	0
W9	$\theta_{19} = -q_5$	130	340	90
P11’	$\theta_{20} = \lambda_5 + q_{11} - q_9 - \lambda_1 + \lambda_3 - 180 + \alpha_7$	200	280	0
W11	$\theta_{21} = -q_{11} + \lambda_5$	130	340	90

Coordinate system according to the above definition and D-H parameters, the pose transformation matrix of coordinate system i relative to coordinate system $i-1$ is established.

$$ {}^{i-1}T_i = \begin{bmatrix} C\theta i & -C\alpha i S\theta i & S\alpha i S\theta i & aiC\theta i \\ S\theta i & C\alpha i C\theta i & -S\alpha i C\theta i & aiS\theta i \\ 0 & S\alpha i & C\alpha i & di \\ 0 & 0 & 0 & 1 \end{bmatrix} \tag{1} $$

Where C stands for cos and S stands for sin.

3.2 Wheel ground contact model considering slip

The contact between the wheel and the seabed surface is shown in Fig. 5. The coordinate system fixed on the seabed surface is established, and the *Xci* axis is defined along the tangent point direction of the contact point, and the *Zci* axis is along the normal direction of the contact point. The coordinate system fixed on the wheel axis is defined at the wheel center of the wheel, R is the wheel radius, *Xwi* axis is in horizontal direction, and *Zwi* axis is in vertical direction. The angle δi between *Zwi* axis and *Zci* axis is defined as contact angle.

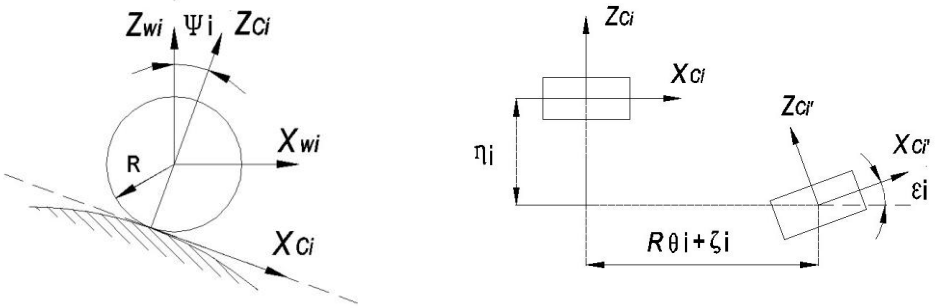

a) Wheel ground contact coordinate system b) Wheel slip coordinate system

Fig. 5. Coordinate transformation model of wheel ground contact

The coordinate transformation matrix between *Wi* -System and *Ci* -system can be obtained by rotation transformation and translation transformation along *Zci* -axis, that is:

$$ {}^{Wi}T_{Ci} = \begin{bmatrix} C\psi_i & 0 & S\psi_i & -RS\psi_i \\ 0 & 1 & 0 & 0 \\ -S\psi_i & 0 & C\psi_i & -RC\psi_i \\ 0 & 0 & 0 & 1 \end{bmatrix} \tag{2} $$

When the wheel *Wi* moves on the ground *Ci* , there may be steering slip εi , lateral slip ηi and wheel rolling slip ζi , the corresponding coordinate transformation matrix is obtained:

$$ {}^{Ci'}T_{Ci} = \begin{bmatrix} C\varepsilon_i & -S\varepsilon_i & S\varepsilon_i & R\theta_i + \zeta_i \\ S\varepsilon_i & C\varepsilon_i & 0 & \eta_i \\ 0 & 0 & 1 & 0 \\ 0 & 0 & 0 & 1 \end{bmatrix} \tag{3} $$

Let $\xi = [\varepsilon, \varsigma, \eta]^T$ be the slip vector.

3.3 Kinematic modeling based on coordinate transformation

According to the definition of the coordinate system, the coordinate transformation chain used to establish the robot motion model is shown in Fig. 6.

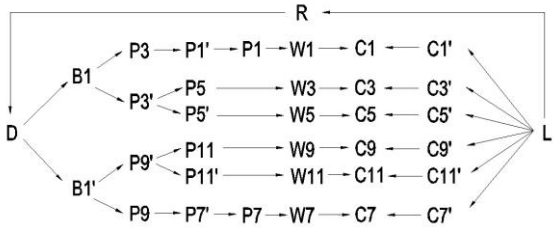

Fig. 6. Coordinate transformation diagram

C_i is the wheel ground contact point coordinate system, Wi is the wheel axis coordinate system, D is the middle section car body coordinate system, R is the reference coordinate system, B_i is the front and rear wheel group hinge point coordinate system, P_i is each joint point coordinate system, L is the seabed surface coordinate system.

According to the car body coordinate system established in Fig. 2 and the coordinate transformation diagram determined in Fig. 4, the position and posture of Wi system relative to the reference coordinate system R at each wheel axis of the robot are as follows:

$$\left.\begin{aligned}
{}^{R}T_{W1} &= {}^{R}T_{D}\,{}^{D}T_{B1}\,{}^{B1}T_{P3}\,{}^{P3}T_{P1'}\,{}^{P1'}T_{P1}\,{}^{P1}T_{W1}\\
{}^{R}T_{W3} &= {}^{R}T_{D}\,{}^{D}T_{B1}\,{}^{B1}T_{P3'}\,{}^{P3'}T_{P5}\,{}^{P5}T_{W3}\\
{}^{R}T_{W5} &= {}^{R}T_{D}\,{}^{D}T_{B1}\,{}^{B1}T_{P3'}\,{}^{P3'}T_{P5'}\,{}^{P5'}T_{W5}\\
{}^{R}T_{W7} &= {}^{R}T_{D}\,{}^{D}T_{B1'}\,{}^{B1'}T_{P9}\,{}^{P9}T_{P7'}\,{}^{P7'}T_{P7}\,{}^{P7}T_{W7}\\
{}^{R}T_{W9} &= {}^{R}T_{D}\,{}^{D}T_{B1'}\,{}^{B1'}T_{P9'}\,{}^{P9'}T_{P11}\,{}^{P11}T_{W9}\\
{}^{R}T_{W11} &= {}^{R}T_{D}\,{}^{D}T_{B1'}\,{}^{B1'}T_{P9'}\,{}^{P9'}T_{P11'}\,{}^{P11'}T_{W11}
\end{aligned}\right\} \tag{4}$$

Therefore, substituting the D-H parameters in Table 1 into the above formula can determine the pose relationship between the wheel center and the reference coordinate system.

The coordinate transformation matrix of the axis Wi of each wheel of the robot relative to the seabed surface is as follows:

$$ {}^{L}T_{Wi} = {}^{L}T_{R}\,{}^{R}T_{Wi} \quad (i = 1 \sim 12) \tag{5}$$

According to the wheel ground contact transformation matrix and wheel ground slip transformation matrix, the instantaneous pose relationship between the vehicle body reference coordinate system and the wheel ground point Ci' coordinate system is established. If the motion state of each wheel on the seabed surface is known, the motion state of the robot can be analyzed. That is

$$ {}^{Ci'}T_{R} = {}^{Ci'}T_{Ci}(\xi i)\,{}^{Ci}T_{Wi}(\delta i)\,{}^{Wi}T_{R}(qi) \tag{6}$$

In order to quantify the motion of the robot, the robot is configured with a velocity vector $\left[\dot{x}\ \ \dot{y}\ \ \dot{z}\ \ \dot{\phi}x\ \ \dot{\phi}y\ \ \dot{\phi}z\right]^{T}$ ($\dot{x}$ is the forward direction speed of the robot, $\dot{y}$ is the lateral velocity of the robot, $\dot{z}$ is the up and down velocity of the

robot, $\dot{\phi}x$ is the yaw angular velocity of the robot, $\dot{\phi}y$ is the pitch angular velocity of the robot, and $\dot{\phi}z$ is the roll angular velocity of the robot).

When the robot reference coordinate system is sliding, the transformation matrix ${}^{R'}T_R = {}^{R'}T_{CWi'}\,{}^{CWi'}T_R$ can be used to describe the pose. Since ${}^{R'}T_{CWi'}$ is independent of time, ${}^{R'}\dot{T}_R = {}^{R'}T_{CWi'}\,{}^{CWi'}\dot{T}_R$.

${}^{CWi'}\dot{T}_R$ represents the transformation matrix between the robot body reference coordinate system and the first wheel grounding point coordinate system. Namely,

$$ {}^{CWi'}\dot{T}_R = \frac{\partial {}^{CWi}T_R}{\partial qi}\dot{q}i + \frac{\partial {}^{CWi}T_R}{\partial ri}\dot{\theta}i + \frac{\partial {}^{CWi}T_R}{\partial \xi i}\dot{\xi}i + \frac{\partial {}^{CWi}T_R}{\partial \delta i}\dot{\delta}i \tag{7} $$

Then according to the definition of matrix transformation differential, the transformation matrix ${}^{R'}\dot{T}_R$ can be obtained, that is

$$ {}^{R'}\dot{T}_R = \begin{bmatrix} 0 & -\dot{\phi}_Z & \dot{\phi}_y & \dot{x} \\ \dot{\phi}_Z & 0 & -\dot{\phi}_X & \dot{y} \\ -\dot{\phi}_y & \dot{\phi}_X & 0 & \dot{z} \\ 0 & 0 & 0 & 0 \end{bmatrix} \tag{8} $$

The Jacobian matrix between the motion of the main body and the motion of each wheel of the compound wheeled walking mechanism is as follows:

$$ \dot{u} = J_{ij}q_j \qquad (i = 1, 2...6;\ j = 1, 2...n) \tag{9} $$

Where $\dot{u}$ is the velocity vector of the car body, q_j is the velocity vector of each joint point, and J_{ij} is the Jacobian matrix from the car body to the wheel. According to the definition of Jacobian matrix, J_{ij} is expressed as:

$$ J_{ij} = \frac{\partial u_i}{\partial q_j} \qquad (i = 1, 2...6;\ j = 1, 2...n) \tag{10} $$

Therefore, the equation of motion can be changed as follows:

$$\begin{bmatrix} \dot{x} \\ \dot{y} \\ \dot{z} \\ \dot{\phi}x \\ \dot{\phi}y \\ \dot{\phi}z \end{bmatrix} = \begin{bmatrix} J_{t1} & J_{t2} & \ldots & J_{tn} \\ J_{n1} & J_{n2} & \ldots & J_{nn} \end{bmatrix} \begin{bmatrix} \dot{q}_1 \\ \dot{q}_2 \\ \ldots \\ \dot{q}_n \end{bmatrix} \tag{11}$$

In the above formula, J_{tn} and J_{nn} represent the linear velocity and angular velocity caused by joint n unit joint velocity respectively.

4. Kinematics Simulation Analysis of Deep Sea Mining Robot

According to the deep-sea unstructured terrain environment, the kinematics simulation model of mining robot based on Adams software is established [15], and the movement analysis and simulation are carried out for 100 seconds under 500 millimeters step vertical obstacle crossing condition. The simulation process of obstacle crossing is shown in Fig. 7.

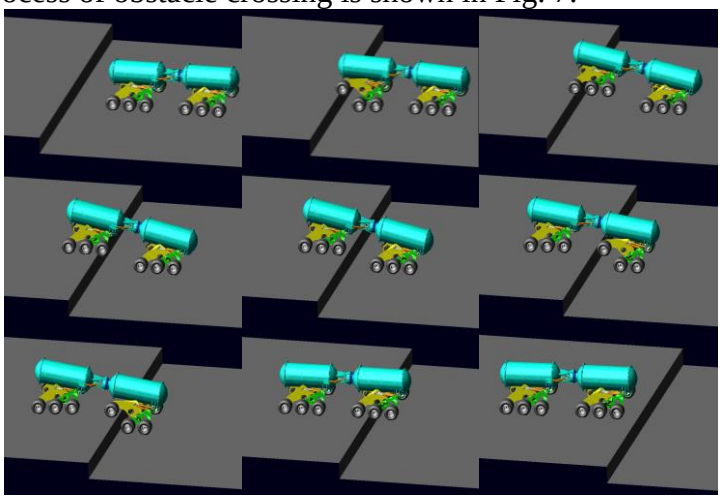

Fig. 7. Robot running a vertical step obstacle

Through the simulation study, the motion curve of the wheel group (as shown in Fig. 8) and the motion curve of the robot Center (as shown in Fig. 9) are obtained respectively.

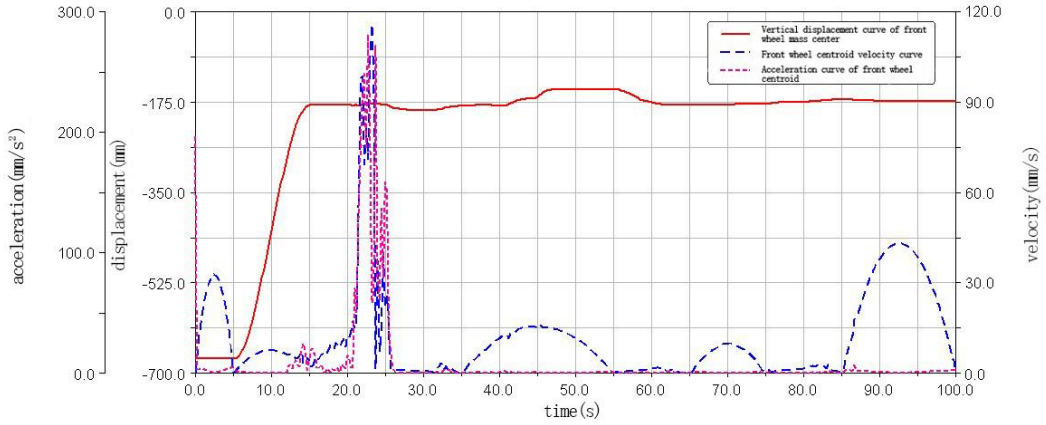

a). Vertical displacement, velocity and acceleration curve of left front wheel

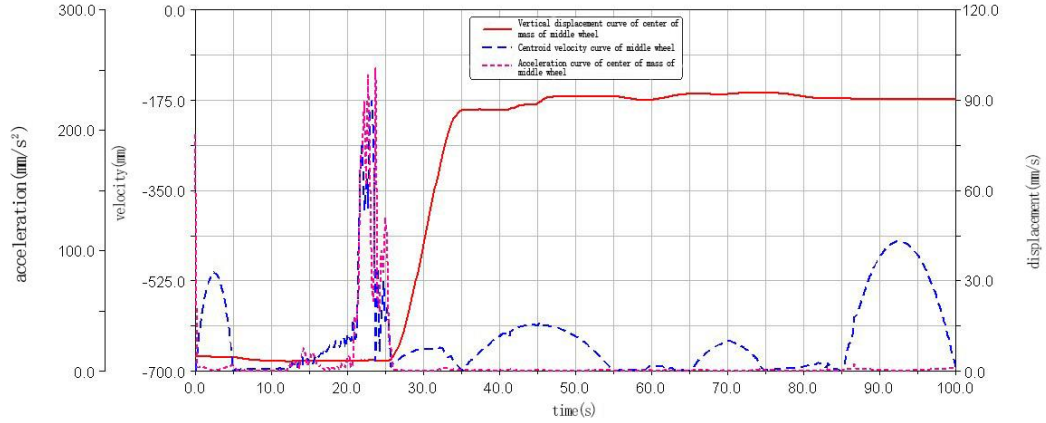

b). Displacement, velocity and acceleration curve of left middle wheel

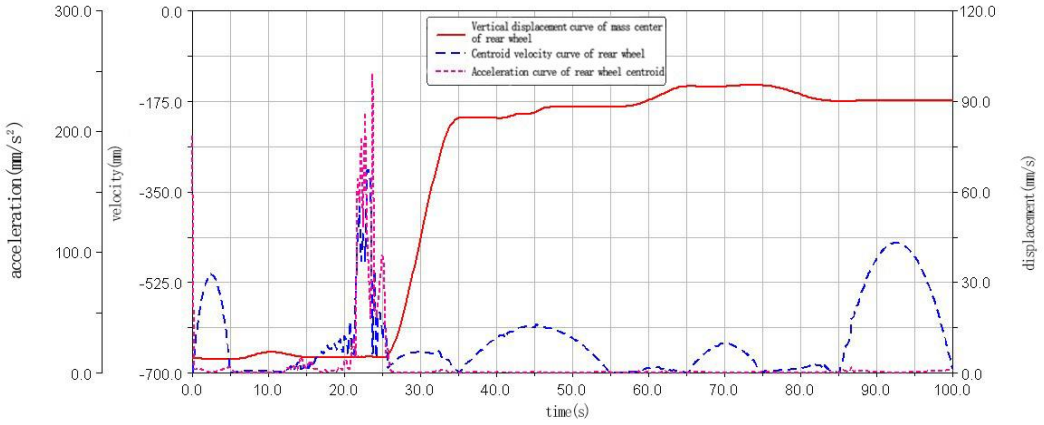

c). Displacement, speed and acceleration curve of left rear wheel

Fig. 8. Simulation curves of robot wheel group motion

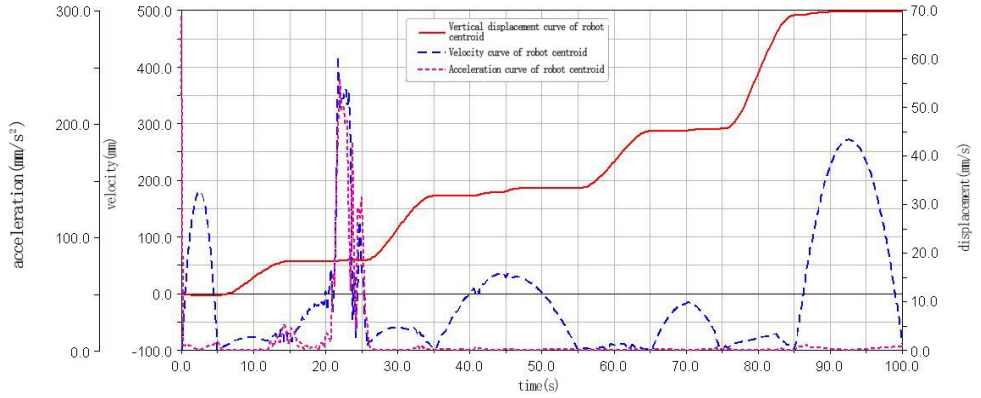

a). Displacement, velocity and acceleration curve of the robot centroid

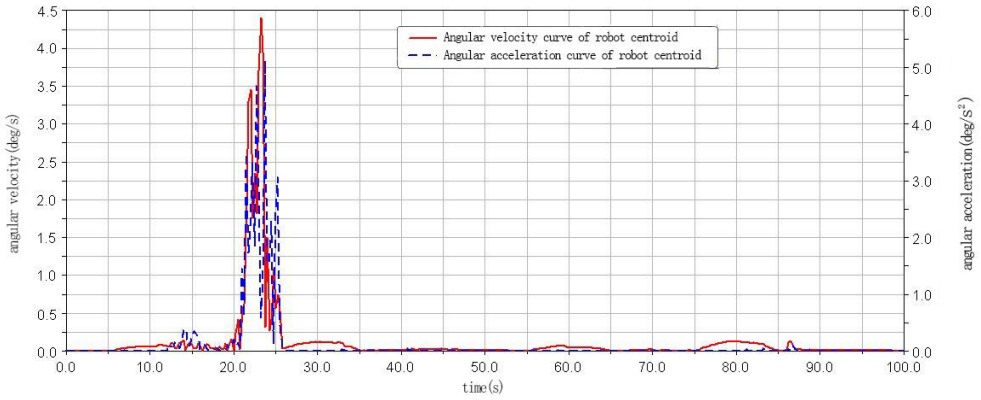

b). Angular velocity and acceleration curve of the robot centroid

Fig. 9. Simulation curves of the robot center motion

Through the simulation curve, it can be seen that in the process of vertical obstacle crossing, the change trend of displacement, velocity and acceleration curve of each wheel group of robot is basically the same:

a) During the process of 0 ~ 5 seconds, the robot stops before the steps, the vertical displacement remains unchanged, while the velocity of the front wheel increases from zero and then decreases;

b) During the process of 5 ~ 15 seconds, the front wheel of the robot is lifted, the vertical displacement increases by 500 millimeters, and the velocity of the front wheel increases from zero and then decreases;

c) During the process of 15 ~ 25 seconds, when the robot reaches the front wheel and steps up, the vertical displacement basically remains unchanged, the velocity of the front wheel increases and decreases gradually, and fluctuates;

d) During the process of 25 ~ 35 seconds, the middle wheel and rear wheel of the robot are lifted up. The center of gravity moves forward due to the rise of

the middle wheel and rear wheel. The vertical displacement of the front wheel is slightly reduced due to the vertical force of the front wheel. The speed of the front wheel should be zero, while the front wheel has the phenomenon of forward or backward due to the instability of the vehicle body;

e) During the process of 35 ~ 47seconds, the middle wheel and the rear wheel of the robot gradually cross the steps. The middle wheel and the rear wheel share a part of the force of the front wheel, which makes the vertical displacement slightly higher and the front wheel speed gradually increases from zero;

f) During the process of 47 ~ 55 seconds, when the front wheel of the robot rear wheel group reaches the step and stops, the vertical displacement is basically unchanged, and the wheel speed of the front wheel gradually decreases from the speed of the last action to zero.

g) During the process of 55 ~ 65 seconds, the front wheel of the robot rear wheel group is lifted. When the center of gravity of the whole vehicle rises, it also moves forward. The force on the front wheel increases, resulting in the vertical displacement decreases. The force on the front wheel becomes larger, resulting in a slight decrease in the vertical displacement. The speed of the front wheel should be zero, while the front wheel moves forward or backward due to the instability of the vehicle body;

h) During the process of 65 ~ 75 seconds, the front wheel of the robot rear wheel group moves to the step and stops, the height of the vehicle center of gravity is basically unchanged, the vertical displacement is basically unchanged, and the front wheel speed increases from zero to gradually decreases;

i) During the process of 75 ~ 85 seconds, the center wheel and rear wheel of the robot rear wheel group are raised, the height of the vehicle center of gravity is basically unchanged, and the vertical displacement is basically unchanged. The front wheel speed should be zero, but the front wheel has the phenomenon of forward or backward due to the instability of the vehicle body;

j) During the 85 ~ 100 seconds , the robot moves forward, the middle wheel and the rear wheel successively climb the steps, the whole robot climbs up the steps and stops, the vertical displacement basically remains unchanged, the front wheel speed increases from zero and gradually decreases to zero, thus the 100 seconds simulation process is finished.

5. experimental verification of kinematic characteristics of deep sea mining robot

5.1 Test device and system

The principle prototype of deep-sea mining robot is developed, and the simulation test platform of mining robot is built to verify the correctness of kinematics analysis and Simulation of mining robot in this paper.

The mining robot test system mainly includes speed test system, displacement test system and oil pressure test system. The interface of the test system is shown in Fig. 10, and the test equipment is shown in Fig. 11.

Fig. 10. Testing system

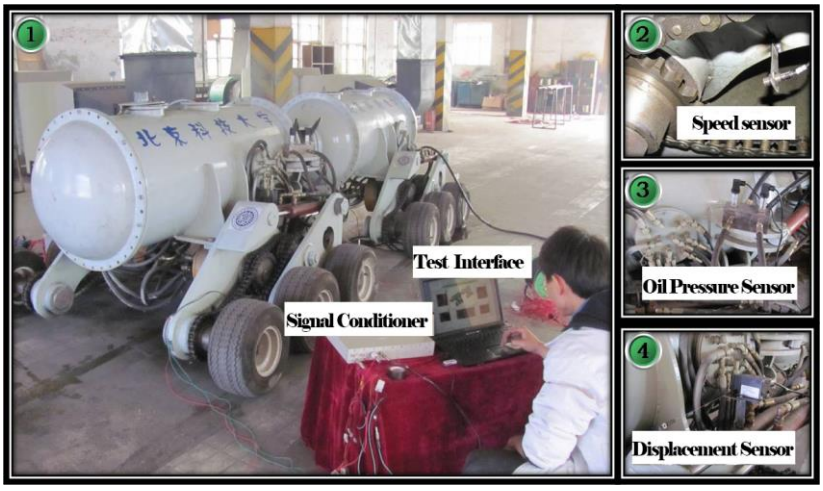

Fig. 11. Test equipment

5.2 Test plan

The characteristics of deep-sea unstructured terrain environment are extracted, and the road test platform is built. The vertical obstacle crossing process is shown in Fig. 12 below.

Fig. 12. Vertical obstacle experiment test

5.3 Test result

The vertical obstacle crossing speed test curve and virtual prototype simulation curve of deep-sea mining robot are shown in Fig. 13.

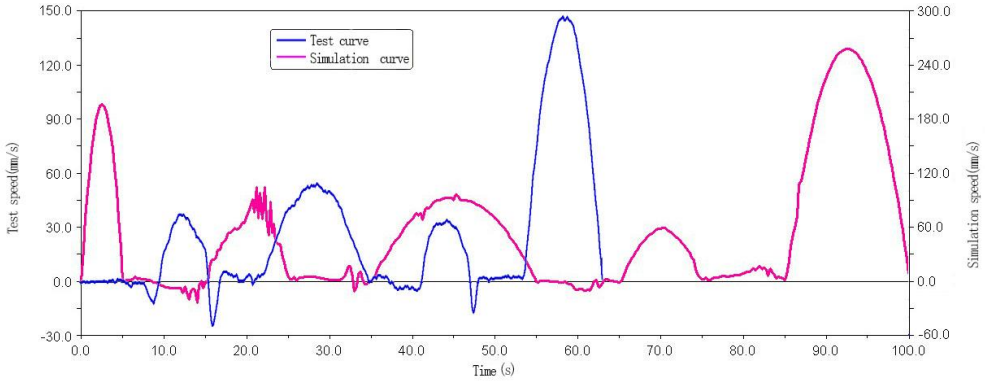

Fig. 13. Comparison curves of velocity test and simulation

Through the comparison and verification of the robot principle prototype test and virtual prototype simulation, it can be seen that the change trend of the speed test curve of the principle prototype is basically consistent with that of the virtual prototype simulation curve, and there are only two small fluctuations at the 16th second and the 47th second. These two moments are the time when the front

wheel of the robot lifts and walks until the middle wheel touches the step, and the theoretical speed at this time should be zero, but the speed of both times is less than zero, indicating that the robot has regressed. This is due to the fact that the prototype of the robot did not stop completely at these two moments, and the middle wheel was impacted when it hit the step, which caused the robot to move backward instantaneously. The instability in the obstacle crossing process has certain adverse effects, which will increase the complexity of the robot's obstacle crossing process control and aggravate the wear of brake and wheel.

6. Conclusions

(1) In this paper, a kinematic modeling method of deep-sea wheeled mining robot is proposed, and the kinematics mathematical model of compound wheeled mining robot in deep-sea unstructured terrain environment is established. The kinematics equation of the robot is deduced, and the position and pose information of the robot are obtained. The theoretical basis for the kinematic characteristics analysis of the deep-sea wheeled mining robot is provided;

(2) The virtual prototype simulation model of the deep-sea mining robot is established, and the vertical obstacle crossing condition in the deep-sea unstructured environment is simulated. The simulation curves of displacement, velocity, acceleration and angular acceleration of the robot are obtained, which provides the basis for the theoretical verification of the kinematics characteristics of the deep-sea mining robot;

(3) The principle prototype of the robot is developed, and the test platform is built to test its vertical obstacle crossing performance. The test results verify the accuracy of theoretical calculation and the effectiveness of simulation analysis, which provides technical support for the actual development of deep-sea composite wheeled mining robot.

(4) Therefore, the kinematic characteristics analysis method of deep-sea composite wheeled mining robot can provide technical support for the exploration and exploitation of deep-sea resources in China. The research results can play an important role in military, explosive disposal, disaster relief, disability assistance, mining, forestry and other aspects, which has important academic significance and engineering application value.

Acknowledgements

This work was financially supported by National key R & D plan (2016YFC0304102).

REFERENCES

[1]. *S. J. Liu, C. Liu, Y. Dai,* "Status and Progress on Researches and Developments of Deep Ocean Mining Equipments", Chinese Journal of Mechanical Engineering, **vol.** 50, no. 2, Jan. 2014, pp. 8-18.

[2]. *S. Kim, S.-G. Cho, M. Lee, et al.*, "Reliability-based design optimization of a pick-up device of a manganese nodule pilot mining robot using the Coandă effect", **vol.** 33, no. 8, 2019, pp. 3665-3672.

[3]. *Y. L. Feng, H. R. Li,* Deep Sea Mineral Resources Development and Utilization. Beijing, China Ocean Press, 2004, pp. 56-78.

[4]. *L. Li, Y. D. Fan, "*Research on characteristics of walking hydraulic system of deep sea mining robot", The Ocean Engineering, vol. 37, no. 6, Nov. 2019, pp. 29-38 .

[5]. *F. B. Qiao, R. Q. Yang,* "Analysis on the stair-climbing ability of six-wheeled mobile robot", Robot, vol. 26, no. 4, 2004, pp. 301-305.

[6]. *X. Y. Deng,* "Kinematic analysis of an omni-directional mobile robot", Robot, vol. 26, no. 1, 2004, pp. 49-53.

[7]. *X. K. Song, D. L. Tan, Z. W. Wu, et al.,* "Kinematics modeling and analyses of all-terrain wheeled mobile robots", Chinese Journal of Mechanical Engineering, vol. 44, no. 6, 2008, pp. 148-154.

[8]. *Z. W. Wang, B. Liang, H. X. Wu,* "Kinematical modeling and analysis of six-wheel lunar rover", Journal of Astronautics, vol. 4, no. 5, 2003, pp. 456-462.

[9]. *P. F. Muir, C. P. Neumann,* "Kinematics Modeling of Wheeled Mobile Robots", Journal of Robotic Systems, vol. 4, no. 2, 1987, pp. 281-340.

[10]. *A. T. Bazilevskiy, N. Grebennik,* "Physical and mechanical properties of lunar soil as function of specifics of relief and processes in vicinity of operation of Lunokhod-2", USSR Report Space 2, 1984, pp. 65-66.

[11]. *X. L. Yu, W. Xia, H. Luo,* "Kinematics Analysis of the Lunar Rover Based on Rocker-bogie Mechanism", J. of Anhui University of Technology, vol. 25, no. 2, 2008, pp. 137-146.

[12]. *M. Hu, Z. Q. Deng, J. G. Tao, et al.,* Modeling and simulation analysis of six wheeled rocker-steering lunar rove, 1st academic conference of China Aerospace society deep space exploration technology Specialized Committee, 2005, pp. 440-444.

[13]. *X. Y. Yu, H. B. Gao, Z. Q. Deng,* "Different kinematics modeling method and analyzing of new lunar rover with eight wheels", Journal of Beijing University of Aeronautics and Astronautics, vol. 35, no. 4, 2009, pp. 457-463.

[14]. *Z. S. Cai, B. R. Hong, Z. H. Wei,* "Kinematics, dynamic analysis and simulation of lunar rover", J. Huazhong Univ. of Sci. & Tech. (Nature Science Edition), vol. 32, Oct. 2004, pp. 35-37.

[15]. *L. P. Chen, Y. Q. Zhang, W. Q. Ren, et al.,* Mechanical System Dynamics Analysis and ADAMS Application. Beijing, Tsinghua University Press, Jan. 2005, pp. 78-80.